RSC Advances

ROYAL SOCIETY OF CHEMISTRY

www.rsc.org/advances

Cite this: DOI: 10.1039/c0xx00000x

www.rsc.org/xxxxxx

ARTICLE TYPE

Adsorption of gaseous elemental mercury with activated carbon impregnated with ferric chloride

Xue Qian Wang, Ping Wang, Ping Ning, Yi Xing Ma, Fei Wang, Xiao Long Guo, Yi Lan

Fe-based modified activated carbon prepared by impregnation was used for adsorbents of Hg^0 purification. The influence of carriers, active components, $FeCl_3$ solution concentration, calcination temperature, were investigated for Hg^0 adsorption purification. The effects of preparation conditions on the adsorbent were characterized by N_2 adsorption-desorption isotherms, scanning electron microscope (SEM), X-ray photoelectron spectroscopy (XPS), X-ray diffraction (XRD) and (FTIR). The samples modified with $FeCl_3$ showed obviously performance for Hg^0 removal, because the chlorine in metal chlorides acts as an oxidant that promotes the conversion of elemental mercury (Hg^0) into its oxidized form (Hg^{2+}). The mechanisms of mercury adsorption onto the Cl-impregnated activated carbon were proposed. The optimal condition for adsorptive purification are Fe^{3+} concentration of 0.15 mol/L, calcination temperature of 300℃ at the adsorption temperature of 40℃ and carrier gas flow rate is 300mL/min.

Introduction

Mercury in coal-fired flue gas generally occurs in three forms [1~5], elemental mercury (Hg^0), gaseous oxidized mercury (Hg^{2+}), and particle-bound mercury (Hgp). Hg^0 is of high concern due to the characteristics of its persistence, neurological toxicity, volatility, bio- accumulation and not readily removed by existing air pollution control devices [6, 7]. So the specific actions to reduce and/or eliminate mercury were required. A promising method for the removal of Hg^0 from coal combustion flue gas is oxidation of Hg^0 to Hg^{2+} which provides a solution to the current dilemma.

Many strategies have been developed to remove Hg^0 from gas, including sorbent adsorption [8], photo-chemical oxidation [9, 10], and the existing pollution control devices [6, 7, 11, 12]. Activated carbon was prepared from an inexpensive and renewable carbon source. The use of activated carbon (AC) is one of the commonly available control technologies for mercury removal. The extended surface area, high adsorption capacity and high degree of surface reactivity of AC, makes it a most widely used as absorbent material [13].

Some commercial AC has shown equilibrium adsorption capacities as high as 3000ug Hg^0/g C [14]. Adsorption using an activated carbon (AC) especially the AC impregnated with S, Cl, Br or I offered great potential for Hg^0 removal in a flue gas [15]. The equilibrium adsorption capacity for some chemically modified AC has been as high as 11,000ug Hg^0/g C [16]. Studies have also shown that chemically treating the activated carbon can enhances the stability of mercury on the surface through the formation of chemical bonds [17, 18]. But the cost of AC for the adsorption of mercury is high, since activated carbon-to-mercury mass ratio of at least 3000-20,000 (C/Hg) can be necessary to achieve 90% Hg removal [14]. Due to the high cost of commercial activated carbons, use of ACs in industrial scale is not economical, and applying a simple and reliable impregnation method modified activated carbon with higher Hg^0 adsorption capacity may bring this cost down greatly. Therefore, for practical utility there is a need for the development of novel catalysts/sorbents that can be used as an alternative to commercially available sorbents and oxidizing agents in order to enhance the performance, regeneration, and also to reduce the operating costs for sorbent injection mercury control systems used at coal-fired power plants at present.

Fly ash samples modified with $FeCl_3$ [19] are promising materials for controlling mercury emissions, and it can enhance the adsorption performance and, the bromide or iodine-modified chitosan could promote the efficiency of Hg^0 capture more or less [20]; Also, the study, finding Thief carbons (TCs) modified with ferric chloride can increase mercury sorption capacities from 21 ug /g to 206 ug /g nearly a ten times increase [21]. A better understanding of the effect of Cl-containing surface functional groups on mercury adsorption is required to accelerate the development of AC injection as a cost-effective method for reducing mercury emissions from coal-fired power plants.

The main objective of this study, therefore, was to study the effect of chemical activation of an AC using ferric chloride on improving elemental mercury adsorption. The simple and reliable impregnation method is used to modify the AC materials with respect to improve their adsorption performance on Hg^0. In addition, the mercury's stability on adsorbent is critical for avoiding Hg^0 secondary pollution when using the AC injection Hg^0 control technology.

All the Hg^0 adsorption experiments with different kinds of ACs were conducted in air environment. Thus, the effect of different surface characteristics of ACs on Hg^0 adsorption was studied without the influence of flue gas composition. It would be helpful for distinguishing the influence of physical process from chemical one on Hg^0 adsorption by AC. Meanwhile, the essential analysis and characterization of adsorbents have been conducted to reveal the possible mechanism of Hg^0 adsorption and conversion on the adsorbents.

2 Experimental details

2.1 Sample preparation

Activated carbon, shell carbon, and two kinds of molecular sieves prepared from commercial coal-derived carbon (Jiulong Fine Chemical Factory, Chongqing, China) were used as adsorbent supports in the experiments. Each carrier was washed 3 times with distilled water to remove soluble impurities on the supports, and dried at 105℃ for 12 h. The samples (2.0 ±0.1 g) were each impregnated with an aqueous $FeCl_3$ solution (0.1, 0.15, 0.2, 0.3 mol/L, 100mL), an aqueous $ZnCl_2$ solution (0.1mol/L, 100mL), an aqueous $NiSO_4.6H_2O$ solution (0.1mol/L, 100mL), an aqueous $Ce(NO_3)_3.6H_2O$ solution (0.1mol/L, 100mL), an aqueous $C_4H_6CoO_4.4H_2O$ solution (0.1mol/L, 100mL).

The pretreated carriers were impregnated with the prepared chemical reagent solution for 12 h before the solution was filtered, and the adsorbent was subsequently dried in an oven at 105℃ for 12 h, and then calcined in a muffle furnace at the temperature of experiment designed for 4h. Finally, the samples were cooled down to ambient temperature and stored in a desiccator until testing.

The actual metal loading amounts for adsorbents are summarized in table 1. The metal loadings on the adsorbents were determined by atomic adsorption spectrometer (spectrAA220FS, Varian Inc.).

2.2 Sample characterizations

The nitrogen adsorption isotherms at 77.35 K were determined on a multi-spot nitrogen adsorption meter NOVA2000e (Quanta chrome Corp.). Scanning electron microscopy (SEM) produced by the Japanese Hitachi electronic and field emission of S4800. EX-350 Energy Dispersive X-ray Micro-analyzer and HORIBA EMAX Energy were used in this work. XRD analysis was conducted on a Rigaku diffraction meter (D/MAX-2200), which was operated under the conditions of 36 kV and 30 mA using Nifiltered Cu Kα radiation (λ=0.15406 nm) at a rate of 2^o/min from $2\theta=20\sim80^o$. Plus, powdered samples were directly analyzed without pretreatment. The instrument X photoelectron spectroscopy (XPS) used America Thermo ESCALAB 250Xi X photoelectron spectroscopy, in which the X-ray source was operated with an Al Kα anode with a photo-energy of hv 1486.6 eV. The core level binding energy of C1s for carbon at 284.8 eV was used as an internal reference for calibration. The FTIR was manufactured by thermo Nicolet Corporation in America, the model is Magna-IR 170.

2.3 Experimental apparatus and methods

Fig.1 shows the schematic diagram of the experimental system. A dynamic Hg^0 permeation device was used to provide a constant feed of Hg^0 concentration using air as the carrier gas. The air was from cylinder gases and precisely controlled by the rotameter. The concentration of mercury was controlled by adjusting the water bath temperature and carrier gas flow rate. The empty bottle was arranged in order to make the gas mixed more evenly.

The Hg^0 concentration in the reactant gas was maintained at about 30mg/m^3 for all experiments (The purpose is to conduct a pilot experiment simulation). The vapor-phase Hg^0 concentration was continuously monitored by a CVAAS (SG921; Jiangfen, China) based on cold vapor absorption spectrometry and was recorded automatically on a computer.

The adsorption occurred in a quartz columnar reactor with 9 mm in inner diameter and 60 mm in length which was placed in the thermostatic water bath which was set to control the reaction temperature. A given amount of adsorbent was inserted in the middle of the column reactor; the reactor was then packed with quartz wool to support the adsorption layer and avoid its loss. It was demonstrated that quartz wool has no ability for elemental mercury capture [22]. The total flux of gas was 300mL/min, the sorbent mass was 2.0±0.1 g in each test and the reaction temperatures was 40℃. The gas stream would flow through silica gel before entering the mercury analyzer in order to remove water vapor. Thus avoid the interference to the detection of mercury concentration and influence the mercury analyzer. At each designated temperature, Hg^0 concentration downstream the adsorbents were recorded after the process had reached equilibrium, which is defined as fluctuation of Hg^0 concentration being no more than 5% for more than 30 min. Finally, the gas stream passed through potassium permanganate solution before exiting to the exhaust hood.

Before flow into the quartz tube, the simulated flue gas was firstly sent through the bypass to the CVASS to determine the initial mercury concentration.

2.4 Hg^0 breakthrough measurements

Each sample was packed in a quartz column and the breakthrough tests were performed with inlet Hg^0 vapor concentration of 30 mg/m^3 at a flow rate of 300 mL/min. The "breakthrough time" is defined as the time required for the Hg^0 outlet concentration to reach 10% of the inlet concentration in the determination of breakthrough curves. After the end of the experiment, the Hg^0 adsorption capacity was calculated with the corresponding integral according to formula (1) under various conditions of the breakthrough curves [23].

$$X = (Qc_0 t - Q\int_0^t c dt) / m \quad (1)$$

Where X is the adsorption capacity in mg/g, m is mass of adsorption in g, Q denotes the flow rate in m^3/min, c_0 and c represent the initial and outlet concentration of Hg^0 in test times in mg/m^3, and t represent the test time in min, respectively, of the breakthrough curves.

3 Results and discussion

3.1 Effects of carriers on Hg^0 adsorption

Figure.2 shows different breakthrough curves of different carriers. 4 kinds of carriers of mercury were employed, including industrial activated carbon (AC), shell carbon, 36H zeolite and Hβ zeolite. The purpose is to determine the optimal carrier. The carrier breakthrough curves for the Hg^0 removal were assessed in dynamic tests at the adsorption temperature of 40℃, flow rate of 300mL/min, bath temperature of 35℃ and entrance concentration of 30mg/m^3.

As can be seen from Fig.2, Adsorption efficiency of each carrier followed a descending order: AC>shell carbon>36H zeolite>Hβ zeolite. Both 36H zeolite and Hβ zeolite had poor removal efficiency, the penetration only rate reached 43%, 56% when the experiment started. The effect of shell carbon was better than two types of zeolite; its efficiency was 19%. Maybe the weak physical

adsorption of Hg^0 taken place on the surface. But AC carrier showed a significant improvement in Hg^0 removal with a breakthrough time of 330 min. The "breakthrough point" was determined to be the point at which the removal efficiency dropped to below 90%. This may be due to it has large specific surface area, stable chemical stability or hydroxyl group it contains, expanding the adsorption performance and changing selectivity of adsorption mercury by activated carbon. Consequently, we choose the industrial activated carbon (AC) as the experiment carrier.

3.2 Effects of modifiers on Hg^0 adsorption

According to the references, we choose several common metal salt (0.1mol/L$FeCl_3$, $ZnCl_2$, $NiSO_4.6H_2O$, $Ce(NO_3)_3.6H_2O$, $C_4H_6CoO_4.4H_2O$ modify the activated carbon, considering the effect of metal cations on mercury adsorption. Activated carbon modified denoted as Fe/AC, Zn/AC, Ni/AC, Ce/AC, Co/AC, the adsorption breakthrough curves of mercury as shown in figure 3. As observed from figure 3, relatively low concentration of these impregnates had a certain beneficial activation effect for AC; The Fe/AC had the conspicuous removal efficiency, it's adsorption effect was obviously better than Zn^{2+}, Ni^{2+}, Ce^{2+}, Co^{2+} component activated carbon modified and the break-through capacity reached 2.7mg/g. The adsorption capacity of Fe-based modified activated carbon has been greatly improved compared with the pristine sample.

The impregnation of $FeCl_3$ leads to increase in both breakthrough time and the amount of Hg^0 adsorbed by the activated carbon, suggesting that the improvement in the Hg^0 capacity is attributed to the active groups formed after the introduction of $FeCl_3$. That the iron adsorbent has better adsorption effect is because $FeCl_3$ can get even distribution in the surface of AC using developed pore structure and large specific surface area. In addition to physical absorption, also occurred chemical adsorption process strongly [19, 21, 24], Chemical reaction formula is described as follows:

$$2Fe^{3+}+Hg^0 \leftrightarrow Hg^{2+}+2Fe^{2+} \quad (2)$$

$$Fe^{3+}+Hg^0 \leftrightarrow Hg^{+}+Fe^{2+} \quad (3)$$

Fe^{3+} can convert Hg^0 into Hg^{2+}, thereby facilitating the removal of Hg^0 from the flue gas (which has strong oxidative properties). The adsorption effect of $FeCl_3$ impregnated activated carbon was improved significantly, in addition, it equal to infiltration chlorine by impregnated AC using $FeCl_3$, and such can enhance the absorbability for mercury.

Based on the phenomena observed and the analyses available in the literature, the mechanism of chemisorptions of elemental mercury onto the Cl-impregnated activated carbons was proposed as follows. During impregnation, the Cl surface complexes were formed [21]:

$$FeCl_3+ C_nH_xO_y \leftrightarrow Fe^{3+} + [Cl_3\text{-}C_nH_xO_y]^{3-} \quad (4)$$

These Cl-contained functional groups accounted for the chemisorptions of Hg^0 through the following reactions [21]:

$$Hg^0+ [Cl]^- \longrightarrow [HgCl]^+ +2e \quad (5)$$

$$HgCl+2[Cl]^- \longrightarrow [HgCl_2]+2e \quad (6)$$

The reaction (5) can occur at room temperature [25] in the temperature range of 25~140℃ because the Gibbs free energy of the gaseous reaction is very low [26]. Hg^0 combined with chlorine atoms that release from adsorbent surface formation HgCl (g), and then part of formation $HgCl_2$.

The possible oxidative groups, Fe^{3+}, Cl^{-1} and others remained on the surface after impregnated treatment may oxidize Hg^0 during the Hg^0 adsorption process and resulting in the higher Hg^0 sorption capacity of the Fe/AC.

A further research is needed to detect these Cl-contained functional groups using advanced surface characterisation techniques.

3.3 Effects of Fe^{3+} impregnation concentration

The active component concentration is one of the important factors that affect purification effect in the process of preparing adsorbent. The effects of different Fe^{3+} impregnation concentration on purification performance of activated carbon were researched. The results are shown in figure 4. As seen, 0.15mol/L is the best impregnation concentration. The adsorption efficiency of modified activated carbon was influenced by the concentration of $FeCl_3$, in the sequence 0.15mol/L> 0.10mol/L> 0.20mol/L> 0.30mol/L>AC. The corresponding breakthrough capacity was 3.642mg/g, 2.6983mg/g, 2.0230mg/g, 1.8879mg/g, 1.4840mg/g, which changes with the impregnation concentration. The concentration of Fe^{3+} was low so cannot provide sufficient reaction active center. According the X-ray diffraction analysis, it can prove that high concentration will cause the adsorbent micropore blockage and the specific surface area decreased, the 616.3994 m²/g BET of Fe/AC (0.30mol/L) is lower than the value measured for the Fe/AC (0.15mol/L), i.e. 650.1628 m²/g and the pore volume is lower for modified activated carbon (0.342323 cm³/g) than for AC (0.369213 cm³/g). It is well known that the properties of adsorbents are related to their porous structure. The adsorbent micropore blockage will increase pore diffusion resistance of gas-solid reaction or lead to Fe3+ aggregation due to overabundance. Finally, it causes the inhibition of modified activated carbon and reduces combining probability between Hg0 and active site.

Fig.4 Breakthrough curves of Hg^0 on different concentration of Fe^{3+} loading activated carbon (Hg^0 entrance inlet concentration is 30mg/m³, calcination temperature is 300℃).

3.4 Effects of calcinations temperature

When the concentration of $FeCl_3$ is 0.15mol/L, the Hg^0 adsorption breakthrough curves in the calcinations temperature of 200～500℃ are shown in figure 5. The adsorbents denoted as Fe/AC-200, Fe/AC-300, Fe/AC-400 and Fe/AC-500 were prepared in the same manner as previously described except the difference of calcination temperature.

Calcination modified activated carbon is one of the key factors in the preparation process; it can affect crystalline grain distribution activation, pore volume, porosity, pore size distribution and stability of modified carbon. As can be seen from Fig.5, it is disadvantageous for Hg^0 purification when the calcination temperature is too low or too high. The adsorption efficiency under different temperature is in the sequence Fe/AC-300>Fe/AC-400>Fe/AC-500> Fe/AC-105> Fe/AC-200 (the concentration of $FeCl_3$ is 0.15mol/L and dried in an oven at 105

℃). It's not enough to make the active component surface changes and difficulty in forming the active group of effective when temperature is low. On the contrary, it may lead to sintering of active ingredient, adsorbent particles aggregation. Moreover, it may pyrolytic carbon and then destroy the pore and pore structure which result in reducing the specific surface area and further affect adsorptive properties of modified carbon.

It's not good for modified activated carbon adsorption purification for Hg^0, when the calcination temperature is greater than 300℃. This suggests the adsorption effect was the best and active materials get most of active carbon at 300℃. With the increase of calcination temperature, purification effect began to decline. Probably because active substances decompose continue and lose activity gradually. Meanwhile, we find a portion of the activated carbon sintering powder in muffle furnace, which indicates that high temperature can make activated carbon occur pyrolysis, carbon and pore surface destruction, lost its carrier function gradually and then result in poor purification effect. Accordingly, the most appropriate calcination temperature is 300 ℃.

3.5 Adsorbent characterization

3.5.1 SEM and EDS analysis

Figure.6 shows SEM image of 0.15mol/L $FeCl_3$ under different calcination temperature. The shape and size of particles can obviously impact the adsorption capacity.

As illustrated in Figure 6, the morphology of Fig 6 b-d was not evidently different. Sheet structure on the surface of activated carbon is more obvious in Fig 6b than the other two SEM image.

Combined with elemental analysis of different samples using EDS(table 2), it is clearly indicated that the main elements of pristine AC is C and O elements, and has a small amount of Al, Si, S, Ca elements, which is mainly caused by the differences and activation process of activated carbon materials. Meanwhile, it is worth noting that Fe was successfully introduced into the AC through modification. It could be found that the molar ratio of Cl and Fe (n_{Cl}: n_{Fe}) was lower than 3:1. The loss of Cl atoms would be due to the following reasons: Cl atoms were bond to inside layer of the support and therefore, could not be detected.

By the previous discussion, we know that the SEM-EDS just determined the surface layer morphology and composition of the samples. Specific mechanism analysis will be discussed further by the following analysis.

3.5.2 Porosity characterization

In order to study the porous structure characteristics of the prepared adsorbents, the N_2 adsorption-desorption isotherm and the BJH pore diameter distribution (inset) of AC, Fe/AC-105, Fe/AC-300 and Fe/AC-300-Hg^0 (means the Fe/AC-300 after adsorption Hg^0 and the same expression corresponding to the corresponding meaning) are shown in Fig.7. Generally, pores are assorted into three categories based on the diameter as micropores (d<2nm), mesopores (2nm<d<50nm) and macropores (d>50 nm).

As can be seen from the inset in Fig.7, the average pore diameter mainly distributed within the range of 2-50nm and partly more than 50 nm, which suggests that the samples comprised mesopores and macropores. It can be seen that fig 7 showed an IV type N_2 adsorption isotherm with an evident hysteresis loop, suggesting the presence of mesopores in ACs. Furthermore, the hysteresis loop shifts in the relative pressure range of 0.4-1.0, a typical characteristic of mesopores structure. It is considered that the position of the inflection point of P/P0 relates to a diameter in the mesopore range, and the sharpness of the step shows the uniformity of the mesopore size distribution. The distributions of pore sizes for the adsorbents show that the majority pore sizes are mainly located in region of 3-4.5 nm, illustrating that these adsorbents were mesopores structures.

It is well known that the properties of adsorbent materials are related to their porous structure. The presence of a large pore size is considered as fundamental for activated carbon materials used in field of sorbents. These pore structures could provide more adsorption sites. Meanwhile, Hg^0 molecules could easily pass through the pore structures and enter into the interior of AC, which is beneficial to improve the amount adsorbed of Hg^0 on AC.

3.5.3 XRD analysis

In order to determine the active components and crystal load structure, we performed X-ray diffraction analysis of modified activated carbon. The characterization results of Fe/AC under different soaking concentration cremated at 300℃ are given in Fig.8.

It is apparent all the samples afford broad diffraction lines that attribute to the common wood activated carbon graphite basal plane at the two theta degree of 26.6°. The weak diffraction peaks could be attributed to graphite crystal (101) surface appearing at the 2θ value of 44°. these are the characteristic diffraction peaks of C, indicating the crystal form of modified activated carbon remained intact.

Another important observation of the XRD analysis for the AC samples is that there are no characteristic peaks of the iron oxide. This is because $FeCl_3$ is too low in concentration on the surface of the AC to be observed. Combination XRD characterization of samples not found the phase diffraction peak of Fe species, we can draw the conclusions of Fe/AC adsorbents in the form of highly dispersed on the surface of the samples. The heating process also appears to have no effect on the sample structure, indicating good thermal stability of AC. Insufficient reaction time for complete conversion of $FeCl_3$ to iron/iron oxide species during the activation process could have contributed to the presence of iron chlorides in the sample.

3.5.4 X-ray photoelectron spectroscopy analysis

Information about the surface of the sorbents (0.15mol/l-Fe/AC calcined at different temperature) after adsorbing mercury was obtained by X-ray photoelectron spectroscopy (XPS) characterization. XPS spectra over the spectral regions Fe2p, Hg4f and Cl2p are displayed in Fig. 9 a, 9 b, 9 c.

As noted in Fig. 9a, Fe/AC-300 has two obvious peaks of Fe2p centered at 711.4 and 725.22eV respectively. Fe/AC-400 has two obvious peaks of Fe2p centered at 712.23 and 725.22eV respectively. But, Fe/AC-500 has almost no peak. The peak that appears at 710.7 eV and 712.7 eV, which belongs to Fe(Ⅱ) $2p_{3/2}$ and Fe(Ⅲ) $2p_{3/2}$, the peak present at 724.3 eV and 726 eV can be assigned to Fe(Ⅱ) $2p_{1/2}$ and Fe(Ⅲ) $2p_{1/2}$, according the XPS analysis, we know the atomic content of Cl is 0.75% and the atomic of Fe is 2.27%. It could be found that the atomic ratio of Cl and Fe (nCl: nFe) was was between 2:1 and 3:1. Thus ratio indicates that Fe exists as mixed valence of +2, +3 valence form in modified adsorbent. The emergence of partial Fe^{2+} may be

caused by formula (2) ~ (3).

The Hg4f lines centered around 102.9, 103.3 and 103.2eV respectively, was significantly higher than the 99.9 eV reference point for Hg^0, indicating that the Hg is oxidized state as shown in figure 9b. This inferred there must be no Hg^0 on the $FeCl_3$-impregnated AC samples and the result was generated the oxidation of Hg^0, changing from the Hg^0 in the gas phase to Hg^{2+} in the adsorbed phase. Thus, oxidized mercury appeared in modified activated carbon could be formed via oxidative processes.

It is confirmed with our XPS characterization results of the $FeCl_3$ modified AC (Fig. 9c), which show the peaks at about 198.5 eV correspond to the Cl bond to Fe^{3+}, while 200.0 eV corresponds to organic Cl[19,27], and the organic Cl is a relevant species because it is the precursor of the formation of mercuric chloride. The reaction mechanism is described as the formula (4):

These results indicated that $FeCl_3$ modified activated carbon can promote the oxidation of mercury effectively.

3.5.5 Infrared spectroscopy analysis

In order to further confirm the Hg^0 adsorption mechanism, the changes of characteristic absorption peaks of the 0.15mol/L-Fe/AC samples before and after Hg^0 adsorption were investigated via FTIR spectroscopy (Fig. 10).

The IR spectra of all the sorbents show three major peaks, located at, 1101.21, 1322.99, 3440.55cm^{-1}. Attribution of these peaks is generally believed that: the absorption peak of 1101.21cm^{-1} is ascribed to the stretching vibration of phenolic hydroxyl, the absorption peak at 1322.99cm^{-1} is assigned to the phenol, or the stretching vibration of C-O-C and C-O; the absorption peak of 3440.55cm^{-1} attributable to the stretching vibration of the OH in sample surface absorption and the OH of chemical adsorption.

For the Fe/AC-300, Fe/AC-400, Fe/AC-500 samples, the bands at about 1564.06, 1558.28, 931.5 and 829.28 cm^{-1} were attributed to carboxyl groups, carboxyl groups, and the emergence of ether and lactone compound. The IR spectra of the sorbents (Fe/AC-300, Fe/AC-400,) are similar, but the Fe/AC-500 changed greatly under calcinations temperature of 300℃. In the case of after Hg^0 adsorption, the vibration at 1795.49 and 873.64, 1558.28 and 1801.28cm^{-1} (presented due to C=O, O-H, carboxylic acid respectively) have been obvious diminished. This may result from the involvement of corresponding functional groups in Hg^0 adsorption, thus leading to a change of intensity of functional groups. Interestingly, we also found the absorption peak of the sorbents have a similar trend. Simultaneously, it can be found that the calcinations temperature is one of the important factors affecting the carbon surface functional groups. It is more beneficial to promote the formation of the carbonyl group when calcinations temperature is 300℃. That may be one reason why Fe/AC-300 is the best adsorbent and Fe/AC-400 also has good adsorption effect. As is well known, the activated carbon itself can provide active sites for Hg^0 bonding [28] and possessing a high adsorption capacity. So, these functional groups are favorable mercury oxidation to a certain extent.

Conclusions

Activated carbon modified by impregnation, especially by $FeCl_3$ impregnation, has exhibited significantly enhanced adsorption purification ability. Because the chlorine in metal chlorides acts as an oxidant that raises the percentage of oxidized form (Hg^{2+}). The reaction mechanisms of mercury adsorption onto the $FeCl_3$ impregnated activated carbon were proposed.

The impregnation concentration and calcination temperature play important roles in the Hg^0 removal by $FeCl_3$. Fe/AC-300 shows a breakthrough capacity of 3.642 mg Hg^0/g adsorbent at 40℃ and carrier gas flow rate at 300mL/min. The optimum conditions were chosen as impregnation concentration 0.15mol/L, calcination temperature 300℃. 0.15-Fe/AC displays a decreasing sorption capacity with increasing calcination temperature.

$FeCl_3$ impregnated with simple steps, modification reagent needed a low price, and have great potential application in coal-fired flue gas mercury control aspects.

Ackonwledgments

This work was supported by the National Natural Science Foundation of China (No. 51268021, No. 51368026, U1137603), 863 National High-tech Development Plan Foundation (No. 2012AA062504) and by Applied Basic Research Program of Yunnan (No. 2011FB027, No. 2011FA010).

Notes and references

[a] *Kunming University of Science & Technology, NO. 727, Jinming South Road, Chenggong new District, kunming, yunnan,China 650500 Fax: 0871 Tel: 13888183303; E-mail: xqwang214@163.com*

[b] *Kunming University of Science & Technology, NO. 727, Jinming South Road, Chenggong new District, kunming, Yunnan, China 650500 Fax: 0871 Tel: 18314562953; E-mail:wangping214080@163.com*

1. Granite, E. J.; Myers, C. R.; King, W. P.; Stanko, D. C.; Pennline, H. W. Sorbents for mercury capture from fuel gas with application to gasification systems. Ind. Eng. Chem. Res. 2006, 45, 4844-4848
2. Yan, N. Q.; Liu, S. H.; Chang, S. G.; Miller, C. Method for the study of gaseous oxidants for the oxidation of mercury gas. Ind. Eng. Chem. Res. 2005, **44**, 5567-5574.
3. Cao, Y.; Gao, Z. Y.; Zhu, J. S.; Wu, Q. H.; Huang, Y. J.; Chiu, C. C.; Parker, B.; Chu, P.; Pan, W. P. Impacts of halogen additions on mercury oxidation, in a slipstream selective catalyst reduction (SCR), reactor when burning sub-bituminous coal. Environ. Sci. Technol. 2008, **42**, 256-261.
4. Liu, S. H.; Yan, N. Q.; Liu, Z. R.; Qu, Z.; Wang, H. P.; Chang, S. G.;Miller, C. Using bromine gas to enhance mercury removal from flue gas of coal-fired power plants. *Environ. Sci. Technol*. 2007, **41**, 1405-1412.
5. C.L. Senior, J.J. Helble, A.F. Sarofim, Emissions of mercury, trace elements, and fine particles from stationary combustion sources. *Fuel Process. Technol*. 2007, **88** (8), 749-758.
6. Lihui Tian, Caiting Li*, Qun Li,Guangming Zeng, Zhao Gao, Shanhong Li, Xiaopeng Fan. Removal of elemental mercury by activated carbon impregnated with CeO_2. *Fuel.* 2009, 88, *Fuel Process. Technol*. 2000, **65** 263-288.
7. Juan Wang[1], Wenhua Wang[1,*], Wei Xu[1], Xiaohao Wang[1], Song Zhao[2]. Mercury removals by existing pollutants control devices of four coal-fired power plants in China. *Journal of Environmental Sciences.* 2011, **23**(11), 1839-1844.
8. Pavlish, J. H.; Sondreal, E. A.;Mann,M.D.; Olson, E. S.; Galbreath, K. C.; Laudal, D. L.; Benson, S. A. State Review of Mercury Control Options for coal-fired power plants. *Fuel Process. Technol*. 2003, **82**, 89-165.
9. Vidic RD, Siler DP. Vapor-phase elemental mercury adsorption by activated carbon impregnated with chloride and chelating agents. *Carbon.* 2001, **39**, 3-14.
10. Granite EJ, Pennline HW, Hoffman JS. Effects of photochemical formation of mercuric oxide. *Ind Eng Chem Res.* 1999, **38**, 5034-7.
11. McLarnon CR, Granite EJ, Pennline HW. The PCO process for photochemical removal of mercury from flue gas. *Fuel Process Technol.* 2005, **7**(1), 85-9.

12. Chengli Wu[1,2,*], Yan Cao[2], Zhongbing Dong[1].Evaluation of mercury speciation and removal through air pollution control devices of a 190 MW boiler. *Journal of Environmental Sciences*. 2010, **22**(2), 277-282.
13. Fumitake Takahashi[a,*], Akiko Kida[b], Takayuki Shimaoka[a]. Statistical estimate of mercury removal efficiencies for air pollution control devices of municipal solid waste incinerators. *Science of the Total Environment*. 2010, **408**, 5472-5477.
14. Chen S, Rostam-Abadi M, Chang R. Mercury removal from combustion flue gas by activated carbon injection: mass transfer. Pap-Am Chem Soc, *Div Fuel Chem*. 1996, **41**, 442-6.
15. Karatza D, Lancai A, Musmarra D, Zucchini C. Study of mercury adsorption and desorption on sulfur impregnated carbon. *Exp Therm Fluid Sci*. 2000, **21**, 150-5.
16. H. Yang, Z. Xu, M. Fan, A.E. Bland, R.R. Judkins, Adsorbents for capturing mercury in coal-fired boiler flue gas, *J. Hazard. Mater*. 2007, **146**, 1–11.
17. Tseng, R.L, Tseng, S.K. Pore structure and adsorption performance of the KOH-activated carbons prepared from corncob. *J. Colloid Interf. Sci*. 2005, **287**, 428-437.
18. Z. Luo, C. Hu, J. Zhou, K. Cen, Stability of mercury on three activated carbon sorbents. *Fuel Process.* Technol. 2006, **85**, 679-685.
19. Wenqing Xu[1], Hairui Wang[1,2], Tingyu Zhu1[*], Junyan Kuang[1,2], Pengfei Jing1. Mercury removal from coal combustion flue gas by modified fly ash. *Journal of Environmental Sciences*. 2013, **25**(2) 393-398.
20. Anchao Zhang,[†] Jun Xiang,[*,†] Lushi Sun,[†] Song Hu,[†] Peisheng Li,[‡] Jinming Shi,[†] Peng Fu,[†] and Sheng Su[†]. Preparation, Characterization, and Application of Modified Chitosan Sorbents for Elemental Mercury Removal. *Ind. Eng. Chem. Res*. 2009, **48**, 4980-4989.
21. Rodolfo Abraham Monterrozo[1], Maohong Fan, M.ASCE[2], and Morris D. Argyle[3]. Adsorption of Mercury with Modified Thief Carbons. *J. Environ. Eng*. 2012, **138**, 386-391.
22. Li, J. F.; Yan, N. Q.; Qu, Z.; Qiao, S. H.; Yang, S. J.; Guo, Y. F.; Liu, P.; Jia, J. P. Catalytic oxidation of elemental mercury over the modified catalyst Mn/R-Al_2O_3 at lower temperatures. *Environ. Sci. Technol*. 2010, **44**, 426-431.
23. X.Q. Wang, P. Ning, Y. Shi, M. Jiang, Adsorption of low concentration phosphine in yellow phosphorus off-gas by impregnated activated carbon. *J. Hazard. Mater*. 2009, **171**, 588-593.
24. Xu dingmiao. Inorganic Chemistry [M] Beijing people's Medical Publishing House. 1987.(in Chinese)
25. Sliger R, Kramlich J, Marinov N. Towards the development of a Chemical kinetic model for the homogeneous oxidation of mercury by chlorine species. [J]. *Fuel Processing Technology*. 2000, **65**, 423-438.
26. Chase M, Davies C, Downey D, et al. Syverd AN. JANAF thermodynamics tables. [J]. *Journal of Physical and Chemical Reference Data.*1985, **14**:1-1856.
27. Shasha Tao, Caiting Li*****, Xiaopeng Fan, Guangming Zeng, Pei Lu, Xing Zhang, Qingbo Wen, Weiwei Zhao, Diqiang Luo, Chunzhen Fan. Activated coke impregnated with cerium chloride used for elemental mercury removal from simulated flue gas. [J]. *Chemical Engineering Journal* 2012, **210**:547-556
28. Benjaram M. Reddy, Naga Durgasri, Thallada Vinod Kumar & Suresh K. Bhargava. Abatement of Gas-Phase Mercury-Recent Developments. *Catalysis Reviews: Science and Engineering*. 2012, **54**:3, 344-398.
29.

Table 1 Metal loadings for the adsorbent samples.

Sample	Metal loading (mg/L)				
	Fe	Zn	Ni	Ce	Co
Fe/AC	2.11	–	–	–	–
Zn/AC	–	0.003	–	–	–
Ni/AC	–	–	0.286	–	–
Ce/AC	–	–	–	0.004	–
Co/AC	–	–	–	–	1.850

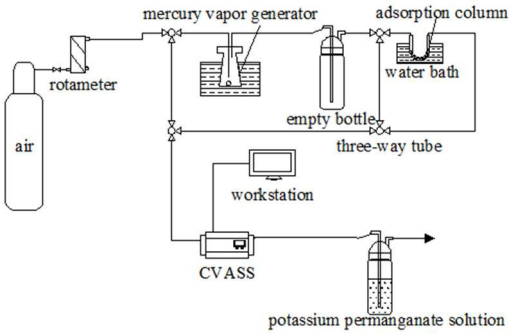

Fig.1. Schematic diagram of the experimental system

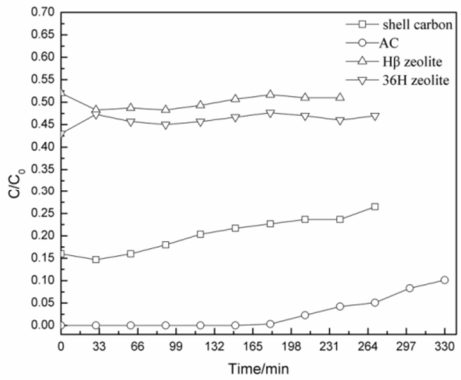

Fig.2 Breakthrough curves of Hg^0 on different supporters at 40℃ (Hg^0 entrance inlet concentration is 30mg/m^3, carriers dried at 105℃).

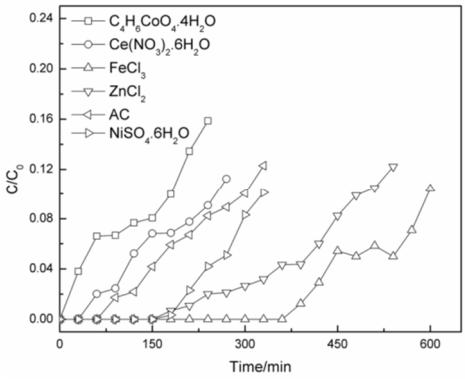

Fig.3 Breakthrough curves of Hg^0 on different impregnated activated carbons(Hg^0 entrance inlet concentration is 30mg/m^3, calcination temperature is 300℃).

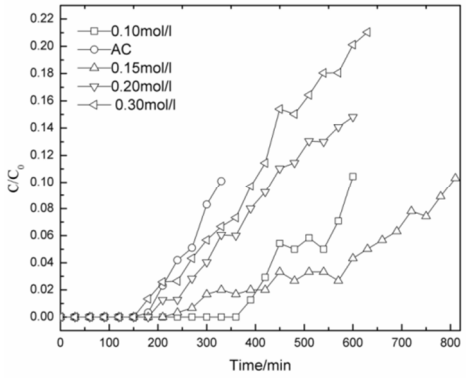

Fig.4 Breakthrough curves of Hg^0 on different concentration of Fe^{3+} loading activated carbon(Hg^0 entrance inlet concentration is 30mg/m^3, calcination temperature is 300℃).

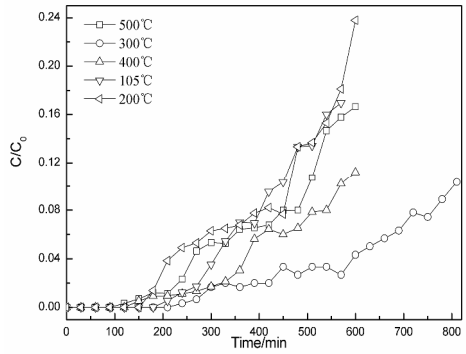

Fig.5 Breakthrough curves of Hg^0 on different calcinated temperatures (Hg^0 entrance inlet concentration is 30mg/m^3).

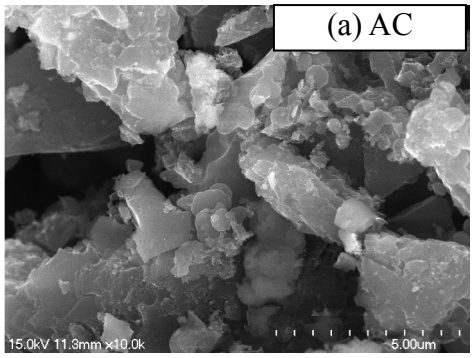

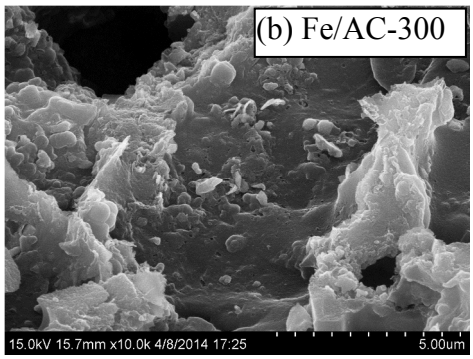

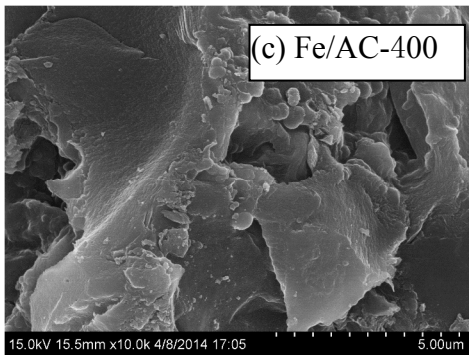

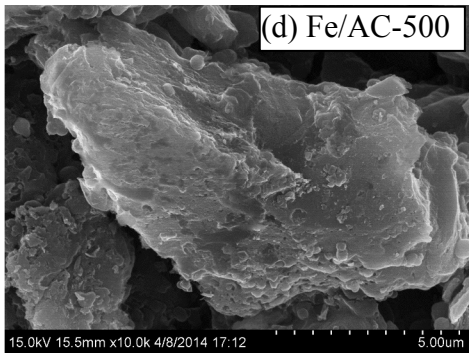

Fig.6 SEM images of surface of AC, Fe/AC-300, Fe/AC-400, Fe/AC-500.

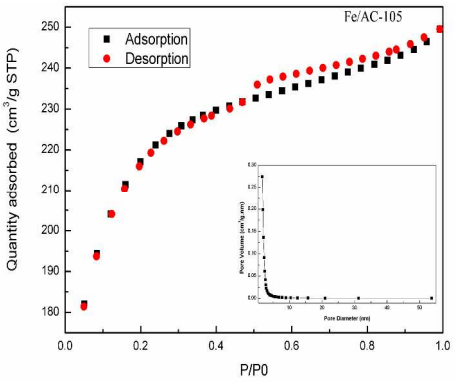

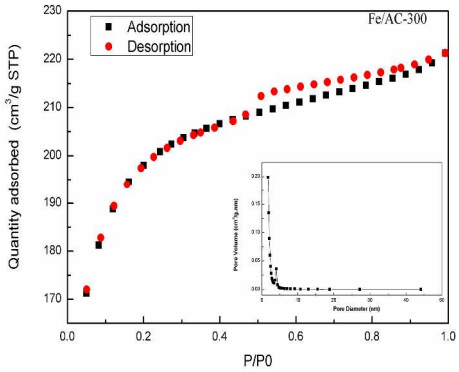

Table 2 Elemental analysis of different samples using EDS.

Sample	Parameters								
		C	O	Si	S	Ca	Al	Cl	Fe
AC	Wt%	86.28	7.25	2.47	0.43	0.69	1.69	0.02	1.17
	at%	91.63	5.78	1.12	0.17	0.22	0.80	0.01	0.27
Fe/AC-300	Wt%	72.5	15.04	2.16	0.86	1.33	1.12	2.48	4.32
	at%	82.57	12.86	1.05	0.37	0.46	0.57	0.96	1.06
Fe/AC-400	Wt%	63.56	24.08	2.02	1.38	1.11	1.89	1.71	3.66
	at%	74.03	21.05	1.01	0.60	0.39	0.98	0.67	0.92
Fe/AC-500	Wt%	76.48	16.53	2.12	0.76	0.73	1.12	0.52	1.39
	at%	83.63	13.57	0.99	0.31	0.24	0.54	0.19	0.33

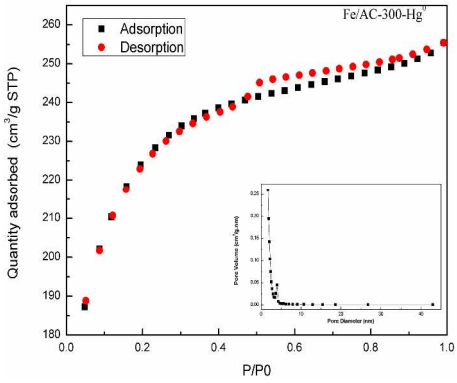

Fig.7 N_2 adsorption-desorption isotherms and pore diameter distributions of AC, Fe/AC-105, Fe/AC-300, Fe/AC-300-Hg^0.

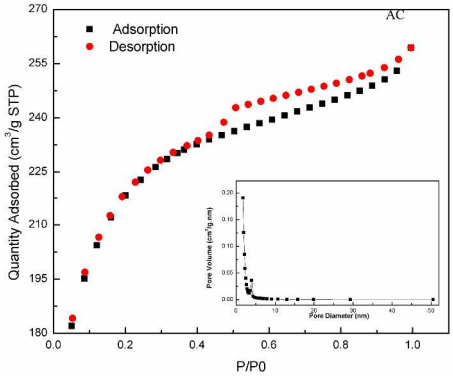

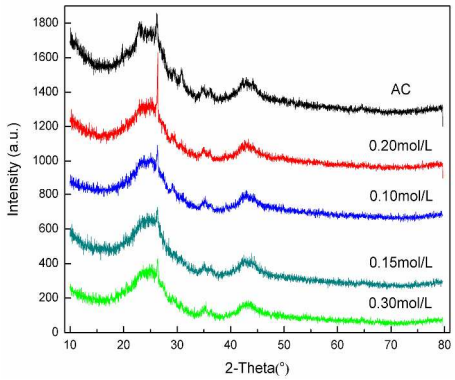

Fig.8 Example of XRD patterns for modified AC.

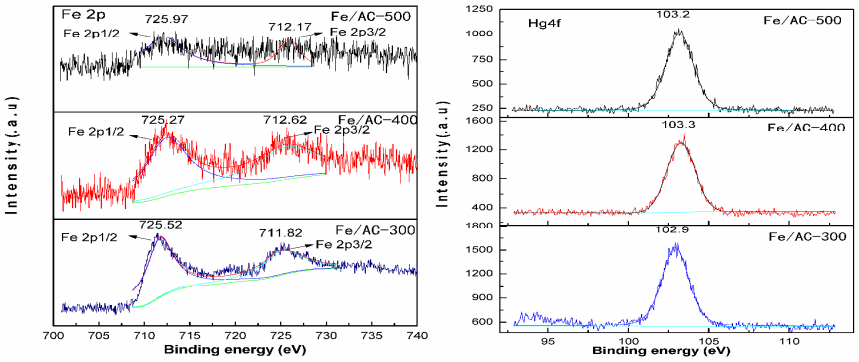

Fig 9 XPS results of the Fe2p(a), Hg4f (b)

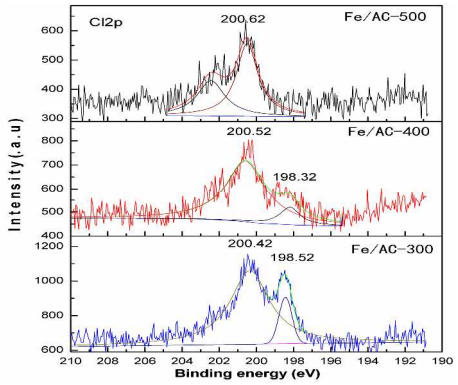

Fig 9 XPS results of the Cl2p(c)

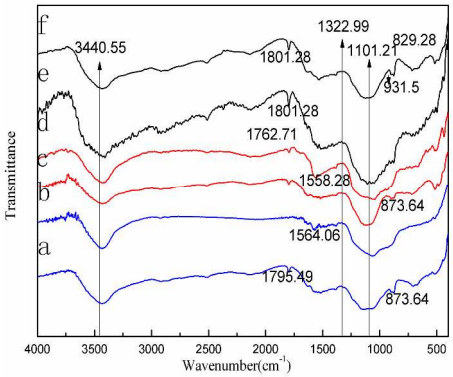

a、Fe/AC-300; b、Fe/AC-300-Hg^0；c、Fe/AC-400；
d、Fe/AC-400-Hg^0；e、Fe/AC-500；f、Fe/AC-500-Hg^0

Fig.10 FTIR spectra of 0.15mol/L $FeCl_3$ calcinated at different temperature before and after adsorption.